Separating traveltimes and amplitudes in waveform inversion

Simon Luo & Dave Hale
Center for Wave Phenomena, Colorado School of Mines, Golden, CO 80401, USA

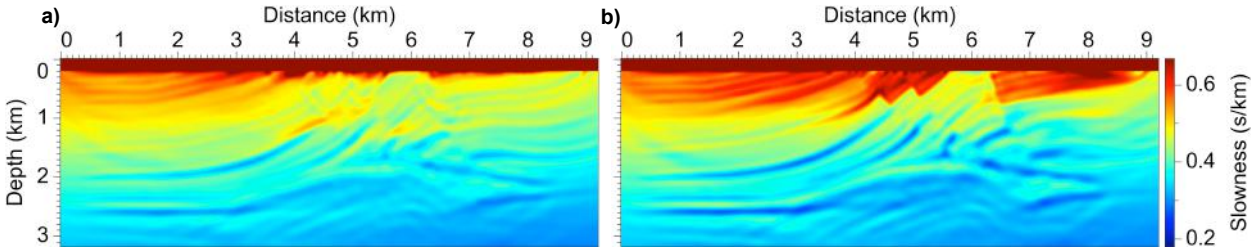

Figure 1. Slowness models computed with (a) conventional full waveform inversion and (b) full waveform inversion using an approximation of the data residual.

ABSTRACT
One difficulty in full waveform inversion is the requirement for an accurate initial model, which if not satisfied, can result in cycle skipping and convergence to local minima. Similarly, in least-squares migration, errors in the background model can lead to an incoherent, defocused image. These difficulties can be attributed in part to the fact that the data residual, the difference between simulated and observed data, contains error in both the smooth background model that affects traveltimes, as well as the rough reflectivity model that affects amplitudes. These two types of error are not treated equally in either full waveform inversion or in least-squares migration. To address this issue, we use an approximation of the data residual to separate traveltime and amplitude errors, and we show that the use of this approximation results in more accurate inversions for velocity in full waveform inversion, and better focused images in least-squares migration.

Key words: waveform inversion least-squares migration traveltime amplitude

1 INTRODUCTION

Iterative migration and inversion algorithms can produce high-resolution images and models of the subsurface. Such algorithms proceed by minimizing an objective function, e.g., a least-squares functional; and various methods exist for solving this optimization problem, including gradient descent and conjugate gradient methods, as well as Gauss-Newton, quasi-Newton, and full-Newton methods. Common to these methods is the computation of the gradient of the objective function with respect to model parameters, which is computed by applying a migration operator (Lailly, 1983; Tarantola, 1984) to a residual that depends on the choice of objective function. Clearly the choice of objective function is important, but from an algorithmic standpoint, the residual is the input to the computation of the gradient. So, it is interesting to investigate the influence of the residual in iterative migration and inversion algorithms.

In full waveform inversion (Lailly, 1983; Tarantola, 1984; Pratt et al., 1998) and least-squares migration (Nemeth et al., 1999; Dai, 2012), with a least-squares objective function, the residual is simply the data residual, i.e., the difference between simulated (modeled) and observed (recorded) data. As shown in Figure 1a, full waveform inversion is susceptible to cycle skipping and convergence to local minima, especially when the ini-

tial model is far from the true model, and simulated and observed data differ by more than one-half cycle. Least-squares migration faces a similar issue when the background velocity model used for migration contains errors, so that traveltimes in the simulated and observed data do not match. These issues arise partly from the fact that nonzero data residuals result from both traveltime and amplitude errors, but the different wavenumber components of the model responsible for these two types of error may be difficult to recover for any one inversion or migration algorithm. For example, least-squares migration inverts for a high-wavenumber reflectivity model; thus, it cannot recover the background model responsible for traveltime errors.

In this report, we use a simple approximation of the data residual when computing the gradient in least-squares migration and full waveform inversion. With this approximation, we can better separate traveltime errors, affected by the low-wavenumber component of the model, from amplitude errors, affected by the high-wavenumber component. We show that this separation can improve focusing and reflector continuity in migration images when the background model contains errors, and, as shown in Figure 1b, that it can also help mitigate cycle skipping and improve convergence in full waveform inversion.

2 LEAST-SQUARES MIGRATION

Migration can be described as the adjoint of a forward modeling operator applied to observed data (Claerbout, 1992). Migration produces a reflectivity image that approximates the true reflectivity insofar as the adjoint of the forward operator approximates the pseudoinverse. Thus, to obtain a more accurate reflectivity image, we require the pseudoinverse of the forward operator.

Least-squares migration (Nemeth et al., 1999; Østmo and Plessix, 2002; Plessix and Mulder, 2004; Kühl and Sacchi, 2003; Dai, 2012) can be described as the pseudoinverse of the forward operator applied to data. Direct application of the inverse operator requires the inverse of the Hessian matrix of second derivatives of an objective function with respect to model parameters, which is prohibitively expensive to compute for most practical-sized problems. Approximations of the inverse Hessian (Gray, 1997; Chavent and Plessix, 1999; Shin et al., 2001; Rickett, 2003; Guitton, 2004; Plessix and Mulder, 2004; Valenciano, 2008; Symes, 2008) are more feasible, and are often used to improve the quality of final migration images or to precondition iterative migration algorithms.

For least-squares migration, we assume a linear relation between data and model parameters. We separate the slowness model $s(\mathbf{x})$ into a smooth background model $s_0(\mathbf{x})$ and a rough reflectivity model

$$r(\mathbf{x}) = s(\mathbf{x})^2 - s_0(\mathbf{x})^2. \tag{1}$$

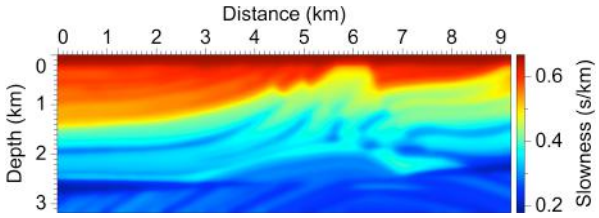

Figure 2. The background slowness model used in Born modeling and least-squares migration.

Then, assuming that wavefields satisfy the acoustic constant-density wave equation, we have, under the Born approximation, two forward modeling equations (Bleistein et al., 2001):

$$\left(s_0(\mathbf{x})^2 \frac{\partial^2}{\partial t^2} - \nabla^2\right) p_0(\mathbf{x}, t; \mathbf{x}_s) = f(t)\delta(\mathbf{x} - \mathbf{x}_s), \tag{2}$$

where $p_0(\mathbf{x}, t; \mathbf{x}_s)$ is the wavefield modeled in the smooth background for a point source with waveform $f(t)$ located at $\mathbf{x}_s$, and

$$\left(s_0(\mathbf{x})^2 \frac{\partial^2}{\partial t^2} - \nabla^2\right) p_1(\mathbf{x}, t; \mathbf{x}_s) = -r(\mathbf{x})\, \ddot{p}_0(\mathbf{x}, t; \mathbf{x}_s), \tag{3}$$

where $p_1(\mathbf{x}, t; \mathbf{x}_s)$ is the wavefield singly scattered by the reflectivity $r(\mathbf{x})$. In equation 3, the wavefield $p_1(\mathbf{x}, t; \mathbf{x}_s)$ is linear in the reflectivity $r(\mathbf{x})$. The solutions of equations 2 and 3 are, respectively,

$$p_0(\mathbf{x}, t; \mathbf{x}_s) = G_0(\mathbf{x}, t; \mathbf{x}_s) * f(t), \tag{4}$$

and

$$p_1(\mathbf{x}, t; \mathbf{x}_s) = -\int G_0(\mathbf{x}, t; \mathbf{x}') * r(\mathbf{x}')\, \ddot{p}_0(\mathbf{x}', t; \mathbf{x}_s)\, d\mathbf{x}', \tag{5}$$

where $G_0(\mathbf{x}, t; \mathbf{x}_s)$ is the Green's function satisfying equation 2 for $f(t) = \delta(t)$. Equation 5 is the Born modeling formula (Bleistein et al., 2001). Note that we do not compute $p_0(\mathbf{x}, t; \mathbf{x}_s)$ and $p_1(\mathbf{x}, t; \mathbf{x}_s)$ from equations 4 and 5, but instead use finite-difference approximations to solve equations 2 and 3.

Given observed data $\tilde{p}(\mathbf{x}_g, t; \mathbf{x}_s)$ recorded at receiver locations $\mathbf{x}_g$, we seek to invert for the reflectivity $r(\mathbf{x})$. We use a conjugate gradient method to minimize an objective function

$$J = \frac{1}{2} \sum_s \sum_g \int \left[p(\mathbf{x}_g, t; \mathbf{x}_s) - \tilde{p}(\mathbf{x}_g, t; \mathbf{x}_s)\right]^2 dt, \tag{6}$$

where $p(\mathbf{x}_g, t; \mathbf{x}_s)$ are the simulated data that depend on the model parameters. The gradient of the objective function in equation 6 with $p(\mathbf{x}_g, t; \mathbf{x}_s) \equiv p_1(\mathbf{x}_g, t; \mathbf{x}_s)$ is (Lailly, 1983; Tarantola, 1984; Plessix and Mulder, 2004)

$$\nabla_r J = -\sum_s \int \dot{p}_0(\mathbf{x}, t; \mathbf{x}_s) \dot{a}_0(\mathbf{x}, t; \mathbf{x}_s)\, dt, \tag{7}$$

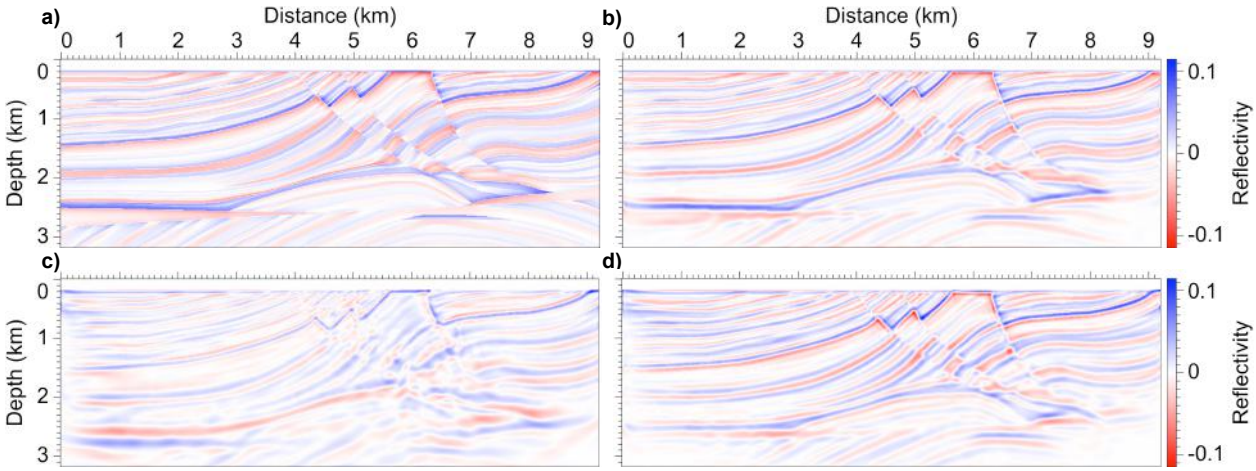

Figure 3. The (a) true reflectivity model, and reflectivity models computed using (b) least-squares migration for the true background slowness, (c) least-squares migration for the true background slowness scaled by 95%, and (d) least-squares migration using the amplitude residual (equation 11) for the true background slowness scaled by 95%.

where $a_0(\mathbf{x}, t; \mathbf{x}_s)$ is the adjoint state variable (Plessix, 2006; Symes, 2007) given by

$$a_0(\mathbf{x}, t; \mathbf{x}_s) = \sum_g G_0(\mathbf{x}, -t; \mathbf{x}_g) * \delta p(\mathbf{x}_g, t; \mathbf{x}_s), \tag{8}$$

where

$$\delta p(\mathbf{x}_g, t; \mathbf{x}_s) = p(\mathbf{x}_g, t; \mathbf{x}_s) - \tilde{p}(\mathbf{x}_g, t; \mathbf{x}_s), \tag{9}$$

are the data residuals. Thus, equation 7 corresponds to a migration of the residuals.

In migration, it is assumed that the smooth background model is correct, and hence that traveltimes in simulated data match those of observed data. If this assumption is satisfied, then any nonzero data residuals (equation 9) are due to differences in amplitude between simulated and observed data, and these differences in turn are due to errors in reflectivity. In this case, least-squares migration can recover an accurate reflectivity model. For example, Figure 3b shows the computed reflectivity model after 20 iterations of least-squares migration using the true background slowness model shown in Figure 2. The background slowness model shown in Figure 2 is obtained by smoothing the true slowness model (Figure 7a) with a two-sided exponential filter that approximates a Gaussian filter with a half-width of 100 m. The data used for migration are computed using 153 shots evenly spaced at the surface with receivers also at the surface, using a 10 Hz source function, which we assume is known. The reflectivity shown in Figure 3b matches well the true reflectivity shown in Figure 3a, because this is the ideal case in which the background slowness model used for migration is the true background slowness.

However, if the background model contains errors, then nonzero data residuals will result from both amplitude and traveltime errors in simulated data. Then, we should expect the image to be degraded, because least-squares migration inverts for reflectivity only. Reflectivity does not directly affect the kinematics of wave propagation, and thus least-squares migration cannot correct for traveltime errors. This degradation can be seen in Figure 3c, which shows the reflectivity model after 20 iterations of least-squares migration using an incorrect background slowness model, specifically, the true background slowness (Figure 2) scaled by 95%. Compared to the reflectivity computed for the true background slowness (Figure 3b), reflectors are misplaced and are generally less focused and less continuous as a result of traveltime errors in the simulated data.

The sensitivity of least-squares migration to errors in the background model has been noted by others (e.g., Dai et al., 2011; Yousefzadeh and Bancroft, 2012), and efforts have been made to reduce this sensitivity. For example, some authors use the flatness of common-image gathers as a regularization constraint in least-squares migration (Gerard Schuster, personal communication). Other approaches might involve data- or model-domain preconditioning to mitigate the effects of large traveltime errors.

We propose a simple approach, which is to modify the data residual used when computing the gradient of the objective function. Our goal in this modification is to distinguish terms in the residual due to amplitude errors from terms due to traveltime errors. With this goal in mind, we expand the observed data $\tilde{p}(\mathbf{x}_g, t; \mathbf{x}_s)$ about time $t + \tau$, where τ are the traveltime shifts between simulated and observed data:

$$\tilde{p}(\mathbf{x}_g, t; \mathbf{x}_s) = \tilde{p}(\mathbf{x}_g, t+\tau; \mathbf{x}_s) - \tau\, \dot{\tilde{p}}(\mathbf{x}_g, t+\tau; \mathbf{x}_s) + O(\tau^2). \tag{10}$$

Then, because we assume in migration that the background model affecting the kinematics of wave propa-

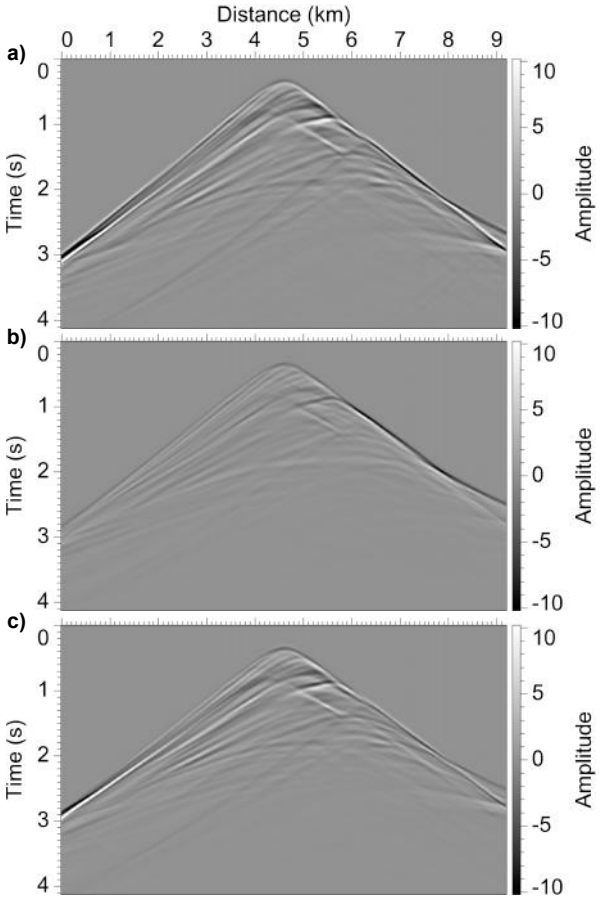

Figure 4. The (a) observed data computed using the true background slowness shown in Figure 2 and true reflectivity shown in Figure 3a for a source located at distance 4.6 km, (b) simulated data computed using the true background slowness scaled by 95% and reflectivity shown in Figure 3c, and (c) simulated data computed using the true background slowness scaled by 95% and reflectivity shown in Figure 3d. Note the similarity in amplitude between the observed data (a) and simulated data (c).

gation is known, i.e., that traveltime shifts τ are small, we drop $O(\tau)$ and higher terms in equation 10, and use

$$\delta p(\mathbf{x}_g, t; \mathbf{x}_s) \approx p(\mathbf{x}_g, t; \mathbf{x}_s) - \tilde{p}(\mathbf{x}_g, t+\tau; \mathbf{x}_s), \qquad (11)$$

for the residual (instead of equation 9) when computing the gradient in least-squares migration. Equation 11 is a poor approximation when the traveltime shifts τ between simulated and observed data are large; however, note that if the traveltime shifts are estimated correctly, then any nonzero residuals in equation 11 are caused by errors in reflectivity. So, it is natural to use equation 11 in least-squares migration since we invert for (only) reflectivity.

We refer to equation 11 as the *amplitude residual*, as it ideally contains only amplitude errors. Computation of the amplitude residual requires estimating the traveltime shifts τ between simulated and observed data. For the examples in this report, we use dynamic warping (Hale, 2013) to estimate these shifts. Compared to local crosscorrelation, dynamic warping is less sensitive to cycle skipping, and estimated shifts are more accurate, especially when the shifts vary rapidly in time.

Figure 3d shows the reflectivity model after 20 iterations of least-squares migration using the amplitude residual (equation 11) to compute the gradient. Compared to the conventional least-squares migration image shown in Figure 3c, reflectors are more continuous and better focused. However, compared to the image for the true background slowness (Figure 3b), we see some discrepancies, most noticeably the mispositioning of reflectors in depth. This mispositioning is not surprising, because the incorrect background slowness model is never corrected in least-squares migration. Therefore, least-squares migration with an incorrect background model will result in misplaced reflectors, along with other migration artifacts. Nevertheless, with least-squares migration using the amplitude residual (Figure 3d), imaged reflectors are more continuous and better focused than for conventional least-squares migration (Figure 3c).

Finally, we compare data modeled using the different reflectivities shown in Figure 3, for a source located at distance 4.6 km. Figure 4a shows the observed data modeled using the true background slowness (Figure 2) and the true reflectivity (Figure 3a), Figure 4b shows the simulated data modeled using the true background slowness scaled by 95% and the reflectivity computed using least-squares migration (Figure 3c), and Figure 4c shows the simulated data modeled using the true background slowness scaled by 95% and the reflectivity computed using least-squares migration using the amplitude residual (Figure 3d). Compared with Figure 4b, the amplitudes in Figure 4c more closely match the amplitudes of the observed data (Figure 4a). However, large traveltime shifts remain between the observed data shown in Figure 4a and the simulated data shown in Figure 4c.

3 FULL WAVEFORM INVERSION

In full waveform inversion (Lailly, 1983; Tarantola, 1984; Pratt et al., 1998), we invert for slowness rather than reflectivity. For this reason, full waveform inversion can potentially recover both high- and low-wavenumber components of the slowness model, and thus can correct for both amplitude and traveltime errors between simulated and observed data.

As before, we solve the acoustic constant-density wave equation

$$\left(s(\mathbf{x})^2 \frac{\partial^2}{\partial t^2} - \nabla^2\right) p(\mathbf{x}, t; \mathbf{x}_s) = f(t)\delta(\mathbf{x} - \mathbf{x}_s), \qquad (12)$$

to model the wavefield $p(\mathbf{x}, t; \mathbf{x}_s)$. Using the same least-

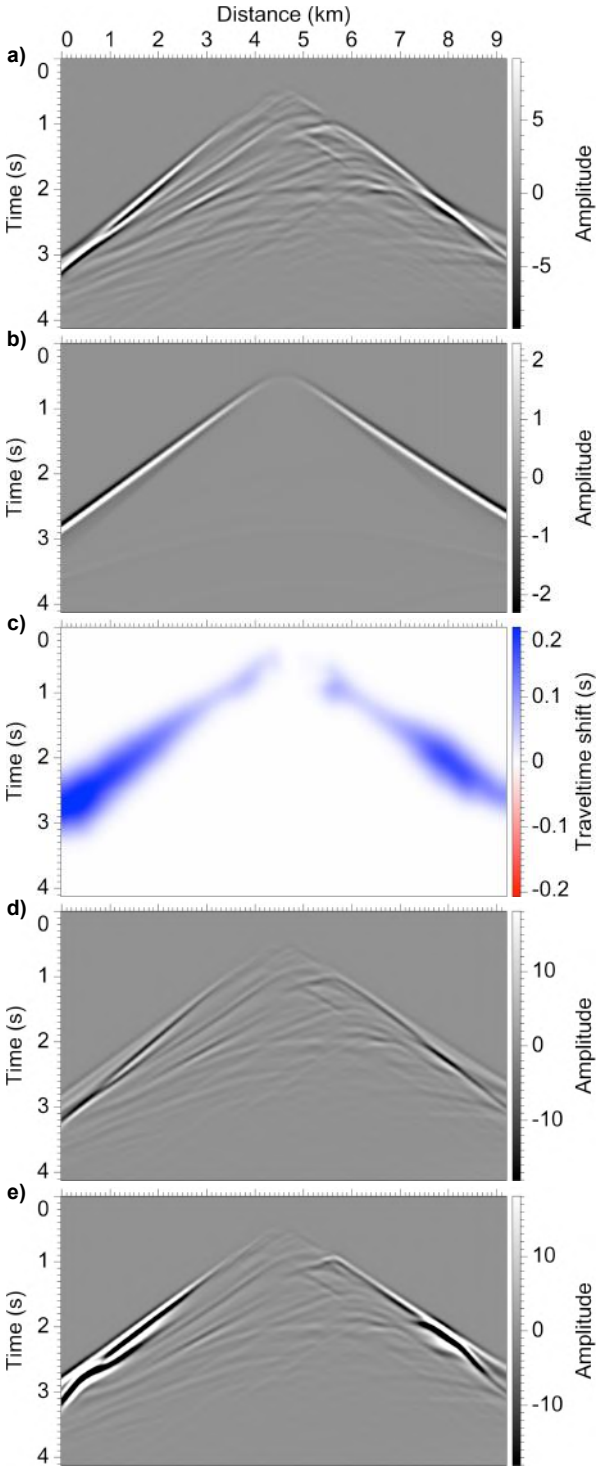

Figure 5. The (a) observed data computed using the true slowness model shown in Figure 7a for a source located at 4.6 km, (b) simulated data computed using the initial slowness model shown in Figure 7b, (c) estimated traveltime shifts between simulated and observed data, (d) data residual, and (e) combined residual.

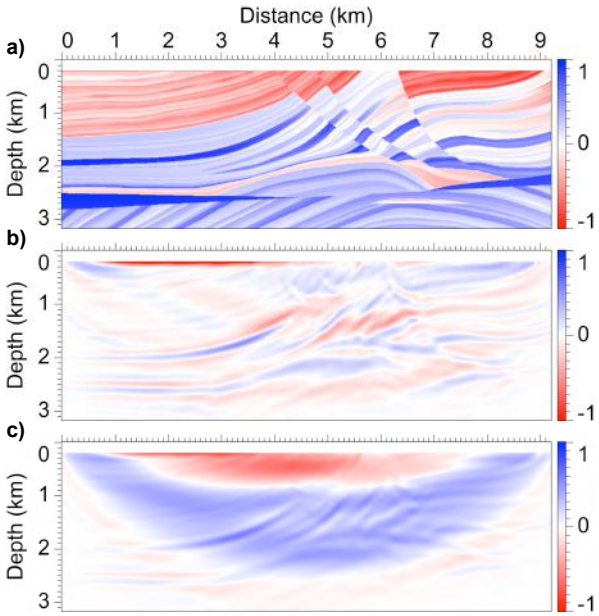

Figure 6. The (a) normalized difference between the initial and true models, (b) gradient for the first iteration of full waveform inversion, and (c) gradient for the first iteration of full waveform inversion using the combined residual (equation 14).

squares objective function (equation 6), the gradient is given by

$$\nabla_s J = -2\, s(\mathbf{x}) \sum_s \int \dot{p}(\mathbf{x}, t; \mathbf{x}_s) \dot{a}(\mathbf{x}, t; \mathbf{x}_s)\, dt, \qquad (13)$$

where $p(\mathbf{x}, t; \mathbf{x}_s)$ and $a(\mathbf{x}, t; \mathbf{x}_s)$ are defined analogously to equations 4 and 8 with $G_0(\mathbf{x}, t; \mathbf{x}_s)$ replaced by $G(\mathbf{x}, t; \mathbf{x}_s)$, the Green's function for equation 12, and likewise for the receiver-side Green's function.

Unlike in least-squares migration, in full waveform inversion we expect both amplitude and traveltime errors between simulated and observed data. For this reason, here we keep the $O(\tau)$ term in equation 10, and thus use

$$\begin{aligned} \delta p(\mathbf{x}_g, t; \mathbf{x}_s) \approx\ & p(\mathbf{x}_g, t; \mathbf{x}_s) \\ & -\tilde{p}(\mathbf{x}_g, t+\tau; \mathbf{x}_s) + \tau\, \dot{\tilde{p}}(\mathbf{x}_g, t+\tau; \mathbf{x}_s). \end{aligned} \qquad (14)$$

for the residual when computing the gradient in full waveform inversion. We refer to this residual (equation 14) as the *combined residual*, since it combines the amplitude residual (equation 11) with a traveltime-like residual.

An example of the combined residual is shown in Figure 5. The source function is a Ricker wavelet with 5 Hz peak frequency. Figure 5a shows the observed data modeled in the true slowness model shown in Figure 7a; Figure 5b shows the simulated data modeled in the initial slowness model shown in Figure 7b; Figure 5c shows the traveltimes shifts between simulated

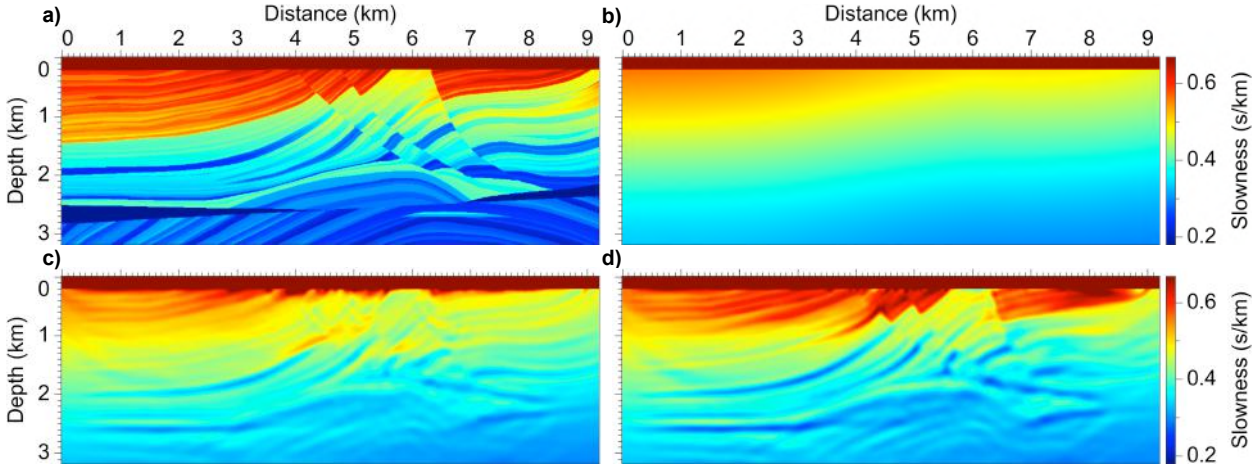

Figure 7. The (a) true slowness, (b) initial slowness, (c) slowness computed with conventional full waveform inversion, and (d) slowness computed with full waveform inversion using the combined residual (equation 14).

and observed data, estimated using dynamic warping; Figure 5d shows the data residual (equation 9); and Figure 5e shows the combined residual (equation 11). Note the similarity between Figures 5d and 5e, except for the early arrivals, which have larger amplitude in Figure 5e because of the large traveltime shifts between the first arrivals in the simulated and observed data. Despite this similarity, however, gradients computed using these two residuals show significant differences.

Gradients computed with 77 shots evenly spaced at the surface and with receivers also at the surface are shown in Figures 6b and 6c. Figure 6a shows the normalized difference between the initial slowness model shown in Figure 7b and the true slowness model shown in Figure 7a, and thus indicates the ideal gradient direction. Figure 6b shows the gradient for the first iteration of full waveform inversion computed using the data residual (Figure 5d), while Figure 6c shows the gradient for the first iteration computed using the combined residual (Figure 5e). Comparing Figures 6a and 6b, notice in some areas the difference in sign, which may result in slow convergence for full waveform inversion. Comparing Figures 6b and 6c, notice that the gradient computed using the combined residual contains more low-wavenumber information. When the initial model is far from the true model, as is the case for this example, the traveltime-like term in the combined residual will tend to dominate due to large traveltime shifts between simulated and observed data. As a result, the gradient will compensate mostly for traveltime errors, hence the low-wavenumber content in the gradient in Figure 6c. Once the kinematics are corrected and the traveltime shifts decrease, the amplitude residual will become more significant, and the gradient will begin to correct for amplitude errors caused by the high-wavenumber component of the model. In this way, the inversion tends to first update the low-wavenumber component of the model before updating the high-wavenumber component.

Figure 7 shows the results of the inversion. Figure 7a shows the true slowness model, which we seek to recover from the initial slowness shown in Figure 7b. Figure 7c shows the computed slowness model after 20 iterations of full waveform inversion, while Figure 7d shows the slowness model after 20 iterations of full waveform inversion using the combined residual (equation 14). Compared to Figure 7c, Figure 7d is closer to the true slowness, especially in shallow areas of the model. The improvement in Figure 7d is most noticeable in shallow areas because it is difficult to use reflection energy to update the low-wavenumber component of the model. To more effectively use reflection energy, one could alternately update the high- and low-wavenumber components of the model (Xu, 2012; Ma, 2012).

4 CONCLUSION

Using an approximation of the data residual, we are able to separate traveltime errors, due to an incorrect background model, from amplitude errors, due to an incorrect reflectivity model. We have demonstrated that the use of this approximation in computing the gradient of the objective function yields more coherent and better focused images in least-squares migration, and more accurate slowness models in full waveform inversion.

The result of using the amplitude residual in least-squares migration is a more focused reflectivity model (migration image), and forward modeling using this reflectivity model produces simulated data that match well the amplitudes of observed data, but not the traveltimes. These remaining traveltime errors indicate that the use of the amplitude residual in least-squares migration does not minimize the difference between simulated

and observed data. However, if our goal is to obtain a focused image, then perhaps minimizing that data difference is not the best approach.

In the case of full waveform inversion, using the combined residual results in a more accurate slowness model. This might suggest that, compared to the data residual, the combined residual minimizes an objective function that is more quadratic and contains fewer local minima. Also worth noting is that if there are no traveltime errors between simulated and observed data, then the combined residual equals the data residual. Thus, full waveform inversion using the combined residual could potentially achieve the same resolution as conventional full waveform inversion, in addition to being less susceptible to cycle skipping and local minima.

One remaining issue is that, because we approximated the data residual without considering the objective function, it is unclear what objective function is being minimized with either the amplitude residual or the combined residual. For small traveltime shifts, our approximation of the data residual is more valid, and the objective function could simply be the least-squares function. But for the examples shown, the traveltime shifts were relatively large. Nevertheless, the use of an approximation of the data residual improved the models computed using least-squares migration and full waveform inversion.

ACKNOWLEDGMENT

This research was supported by the sponsors of the Consortium Project on Seismic Inverse Methods for Complex Structures.

REFERENCES

Bleistein, N., J. K. Cohen, and J. W. Stockwell, Jr., 2001, Mathematics of multidimensional seismic imaging, migration, and inversion: Springer-Verlag New York, Inc.

Chavent, G., and R. Plessix, 1999, An optimal true-amplitude least-squares prestack depth-migration operator: Geophysics, **64**, 508–515.

Claerbout, J. F., 1992, Earth soundings analysis: Processing versus inversion: Blackwell Scientific Publications.

Dai, W., 2012, Multisource least-squares reverse time migration: PhD thesis, King Abdullah University of Science and Technology.

Dai, W., X. Wang, and G. T. Schuster, 2011, Least-squares migration of multisource data with a deblurring filter: Geophysics, **76**, R135–R146.

Gray, S., 1997, True amplitude migration: a comparison of three approaches: Geophysics, **62**, 929–936.

Guitton, A., 2004, Amplitude and kinematic corrections of migrated images for nonunitary imaging operators: Geophysics, **69**, 1017–1024.

Hale, D., 2013, Dynamic warping of seismic images: Geophysics, **78**, S105–S115.

Kühl, H., and M. D. Sacchi, 2003, Least-squares wave-equation migration for AVP/AVA inversion: Geophysics, **68**, 262–273.

Lailly, P., 1983, The seismic inverse problem as a sequence of before stack migration: Conference on Inverse Scattering: Theory and Applications, SIAM, 206–220.

Ma, Y., 2012, Waveform-based velocity estimation from reflection seismic data: PhD thesis, Colorado School of Mines.

Nemeth, T., C. Wu, and G. T. Schuster, 1999, Least-squares migration of incomplete reflection data: Geophysics, **64**, 208–221.

Østmo, S., and R.-E. Plessix, 2002, Finite-difference iterative migration by linearized waveform inversion in the frequency domain: 72nd Annual International Meeting, SEG, Expanded Abstracts.

Plessix, R.-E., 2006, A review of the adjoint-state method for computing the gradient of a functional with geophysical applications: Geophysical Journal International, **167**, 495–503.

Plessix, R.-E., and W. A. Mulder, 2004, Frequency-domain finite-difference amplitude-preserving migration: Geophysical Journal International, **157**, 975–987.

Pratt, G., C. Shin, and G. Hicks, 1998, Gauss-newton and full newton methods in frequency-space seismic waveform inversion: Geophysical Journal International, **113**, 341–462.

Rickett, J. E., 2003, Illumination-based normalization for wave-equation depth migration: Geophysics, **68**, 1371–1379.

Shin, C., S. Jang, and D. J. Min, 2001, Improved amplitude preservation for prestack depth migration by inverse scattering theory: Geophysical Prospecting, **49**, 592–606.

Symes, W. W., 2007, Reverse time migration with optimal checkpointing: Geophysics, **72**, SM213–SM221.

———, 2008, Approximate linearized inversion by optimal scaling of prestack depth migration: Geophysics, **73**, R23–R35.

Tarantola, A., 1984, Inversion of seismic reflection data in the acoustic approximation: Geophysics, **49**, 1259–1266.

Valenciano, A., 2008, Imaging by wave-equation inversion: PhD thesis, Stanford University.

Xu, S., 2012, Full waveform inversion for reflected seismic data: 74th EAGE Conference and Exhibition, Extended Abstracts.

Yousefzadeh, A., and J. C. Bancroft, 2012, Velocity evaluation using least squares prestack migration: 82nd Annual International Meeting, SEG, Expanded

Abstracts.